Trapping and Evolution Dynamics of Ultracold Two-Component Plasmas

J.-H. Choi,* B. Knuffman, X. H. Zhang, A. P. Povilus,† and G. Raithel

FOCUS Center, Department of Physics, University of Michigan, Ann Arbor, Michigan 48109-1040, USA

(Received 14 May 2007; published 28 April 2008)

We demonstrate the trapping of a strongly magnetized, quasineutral ultracold plasma in a nested Penning trap with a background field of 2.9 T. Electrons remain trapped in this system for several milliseconds. Early in the evolution, the dynamics are driven by a breathing-mode oscillation in the ionic charge distribution, which modulates the electron trap depth. Over longer times scales, the electronic component undergoes cooling. Trap loss resulting from $\mathbf{E} \times \mathbf{B}$ drift is characterized.

DOI: 10.1103/PhysRevLett.100.175002 PACS numbers: 52.25.Xz, 37.10.De, 52.27.Aj

Recent developments in atom cooling and trapping have enabled studies of cold-plasma systems. Typically, laser-cooled atoms are photoionized, resulting in plasmas with initial temperatures of the electron and ion components of order 100 K and 1 mK range, respectively [1]. These systems have been studied experimentally [2–4] over a wide range of parameters, such as density and temperature, and many results have been successfully modeled [5–8]. One of the major outstanding goals of the field is to reach the regime of strong coupling, in which the Coulomb interaction energy exceeds the thermal energy of the plasma [1,7,9–11]. Plasma in these exotic liquid or solid forms has already been produced in one-component systems such as laser-cooled ions [12,13]. For the manifestation of strong coupling in two-component plasmas, the trapping of both ionic and electronic components will be critical. The trap studied in this Letter has the unique ability to confine both charged particles and neutral atoms in ground and Rydberg states [14,15]. We envision opportunities to study recombination of ions and electrons in strong magnetic fields, a process important in antihydrogen experiments [16,17]. Finally, the presented methods are generalizable to the large class of atoms which can be laser cooled, creating new possibilities for future cold-plasma research.

In this work, strongly magnetized cold plasmas are confined in a Penning trap with a strong bias magnetic field. The expansion of the plasmas is essentially one-dimensional, leading to confinement times $\gtrsim 1$ ms, which is one to two orders of magnitude longer than that in magnetic-field-free cases. We observe a modulation in the effective electron trapping potential which is caused by space-charge oscillations of the ionic component. Measurements of the electron temperature, conceptually similar to those in [18], reveal that the electron component undergoes cooling.

Our plasmas are produced by photoionization of laser-cooled and magnetically trapped ^{85}Rb atoms at densities up to $\approx 10^9$ cm^{-3} [14]. The magnetic-trapping field has an Ioffe-Pritchard–type geometry with a bias of 2.9 T and a transverse gradient of 0.3 T/cm. The deviation of the magnetic field from cylindrical symmetry is less pronounced than in similar traps [19] and has no measurable effect on the lifetime of the Penning traps used in this work. The plasmas are created in a nested Penning trap [20]; our trap incorporates a quadrupole electric field that is added to the standard Penning-trap magnetic and electric fields. A pair of inner electrodes ($E2$ and $E3$) in Fig. 1 are held at $V_{\text{in}} = -1$ V while outer electrodes ($E1$ and $E4$) are grounded. The calculated electric potential in the axial direction exhibits a local maximum at $z = 0$; this maximum is created by the quadrupole electric field that arises mostly due to the vertical, optical-access apertures in the electrodes [21]. Combined magnetic and electric fields, therefore, produce a trapping potential for both ions and electrons [Fig. 1(b)]. The depth of the trapping potential is tuned by varying V_{in} between -0.5 and -4 V. The variations of the potential away from the symmetry axis are minimal over the transverse extent of the plasma, as shown in Fig. 1(c).

Charged particles, created near $(x, y, z) = (0, 0, 0)$, start to oscillate in the z direction immediately after the creation of the plasma. Assuming approximately symmetric trapping potential $[V(z) \approx V(-z)]$ and initial ion density $[\rho_{i,0}(z) \approx \rho_{i,0}(-z)]$, ions undergo a breathing-type oscillation in the double-well potential within the range $|z| \lesssim 2$ cm, with the oscillation frequency determined by the shape of the outer wells in Fig. 1(b). This differs from the work in Ref. [22], where a sloshing-type oscillation was studied. The electrons undergo oscillations within the electron-trapping range ($|z| \lesssim 1$ cm) of the potential. Since the electron trapping potential is the superposition of the potential due to the electrodes, $E1$–$E4$, and the potential arising from the ionic charge distribution, the modulation of the space-charge density caused by the ionic breathing motion leads to periodic changes in the net electron trapping potential.

We demonstrate the modulation of the electron trap depth by two independent observations. First, we observe a modulation in the electron leak current (Fig. 2). Second, we observe a similar modulation in the strength of the external electric field required to extract the trapped elec-

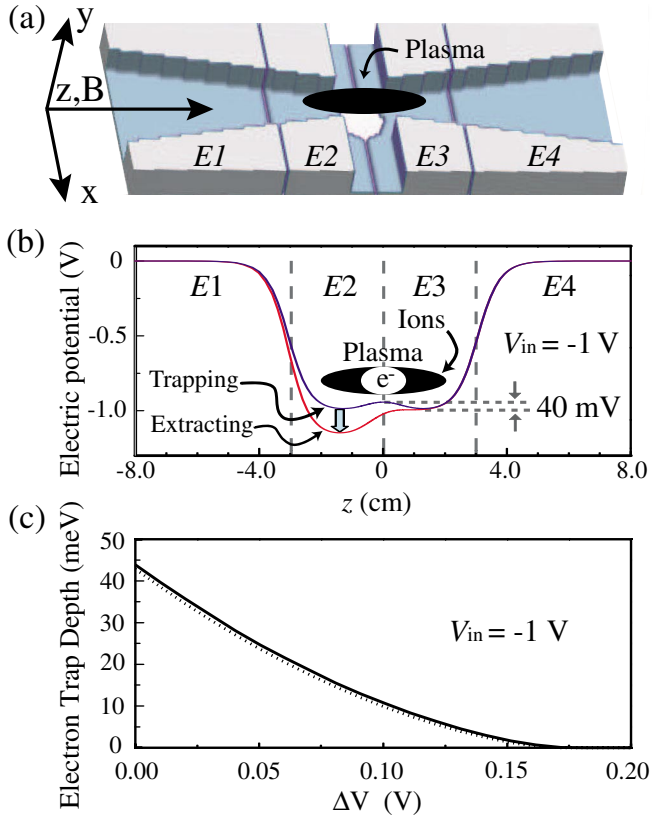

FIG. 1 (color online). (a) Electrodes that generate Penning trap, dc bias, and plasma extraction electric fields. Only the bottom half is shown. (b) Axial electric-potential profile in the two-component plasma trap. To extract electrons from the trap, the voltage on the electrode $E2$ changes in time. (c) Dotted line: Electron trap depth on an axial line through the trap center as a function of the voltage difference ΔV between electrodes $E2$ and $E3$. Solid line: Average electron trap depth sampled by a distribution of electrons $\rho_{e^-}(x, y) = (\pi s^2)^{-1} \exp[-(x^2 + y^2)/s^2]$, where $s = 1.5$ mm.

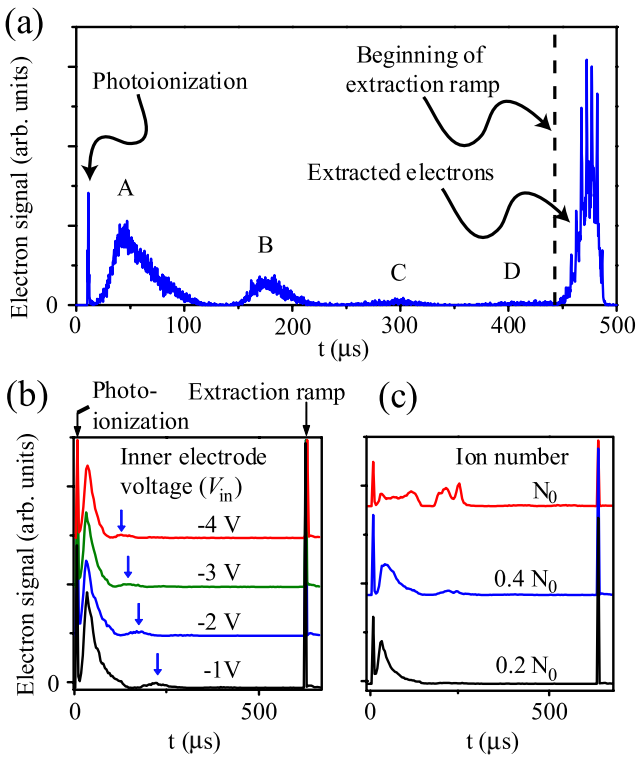

FIG. 2 (color online). (a) Periodic modulation in the electron current due to the ionic motion in the nested Penning trap ($0 < t < 450$ μs). At $t = 450$ μs after photoionization, an applied electric field extracts remaining plasma electrons. (b) The modulation frequency changes as curvature of the Penning-trapping electric potential for ions varies. (c) Effect of the initial ion number on the extraction signal taken under a fixed trap curvature. Initial ion numbers are shown for each signal (N_0 is in the 10^5–10^6 range).

trons (Fig. 3). From these observations, we infer that the ionic component of the plasma is trapped.

To detect the electron current leaking out of the plasma trap, a small dc bias electric field (< 30 mV/cm) is applied to direct electrons to the detector. For $V_{in} = -2$ V with the dc bias field, the electron trap depth is $\gtrsim 50$ meV (600 K). The detected electron leak current exhibits a periodic modulation [peaks A–D in Fig. 2(a)] with a period of ≈ 130 μs, which is consistent with estimated ionic breathing-motion periods in our trap.

To confirm that the modulation observed in Fig. 2(a) originates from the breathing motion of ions, the curvature of the trapping potential has been varied [Fig. 2(b)]. Tighter traps for ions lead to faster modulation of the leak current, indicating the correlation between the ionic motion and the escaping electrons. Even though the trapping potential for the ions is not harmonic, the modulation period follows a $\sqrt{-V_{in}}$ scaling fairly well. The density dependence of the modulation in the electron leak current is studied in Fig. 2(c). With increasing density, the leak current develops complicated, reproducible structures that we believe to be a manifestation of feedback of ionic and electronic space-charge potentials onto the particle motions.

Figure 3 shows the electron signal during the electric-field extraction ramp. The extraction electric field increases stepwise as a function of time, resulting in bursts of electron current at each step. The average arrival time of the extracted electrons (inset in Fig. 3) exhibits a modulation, which provides further evidence of the modulation in the electron trap depth. The modulation period of ≈ 200 μs observed for $V_{in} = -1$ V is consistent with the period of ≈ 130 μs observed for $V_{in} = -2$ V in Fig. 2(a).

The electron extraction signals in Figs. 3 and 4 are used to determine the electron temperatures parallel to the magnetic field direction $T_{\parallel}$. In the temperature calculation, the electron signal is expressed as a function of electron trap depth by first mapping time into ΔV using the dotted curves in Figs. 3 and 4, and then mapping ΔV into electron trap depth using calculations as shown in Fig. 1(c). The results are used to calculate the average energies $\langle E \rangle$ of the trapped electrons. Assuming Maxwell-Boltzmann energy

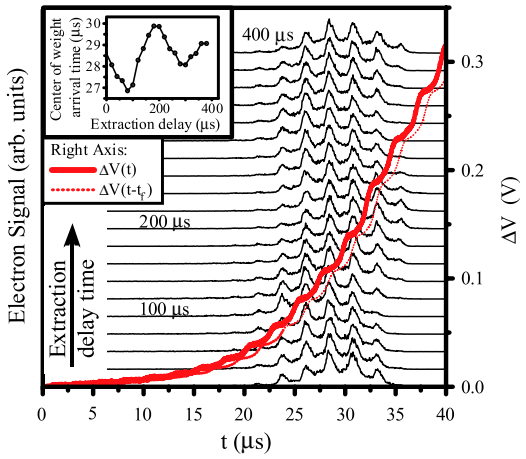

FIG. 3 (color online). Electron signal (left axis) versus time (onset of extraction ramp at $t = 0$) for $V_{\text{in}} = -1$ V and the indicated extraction delay times relative to photoexcitation. The bold curves and the dotted curves show the potential difference ΔV between $E2$ and $E3$ (right axis; t_f denotes time of flight to detector). Inset: Average arrival time versus extraction delay time.

distributions in our one-dimensional potential, the average energies $\langle E \rangle \approx kT_{\parallel}$ (approximate sum of the kinetic and potential energy).

From the distributions in Fig. 3, an electron temperature $T_{\parallel} \approx 250$ K is acquired. The photoexcitation laser has a wavelength of 478.8 nm, which is equivalent to an excess transverse kinetic energy of the photoelectrons of $kT_{\perp} \approx 20$ K. Since the trapped atom cloud has a diameter of a few millimeters, the potential energies of the photoionization products in the axial potential cover a range equivalent to several hundred kelvin, leading to a rapid increase of the longitudinal kinetic energy of the electrons after photoionization. The temperature $T_{\parallel} \approx 250$ K, measured during the first several hundred microseconds after photoexcitation, is consistent with the initial potential energy of the electrons in the electron trapping well. Over a time scale of a few milliseconds, we observe significant electron cooling. In Fig. 4(a), the electron temperature $T_{\parallel}$ is found to drop from 280 to 120 K over the first 1.8 ms; after 3 ms, $T_{\parallel}$ remains approximately constant at about 50 K [Fig. 4(b)].

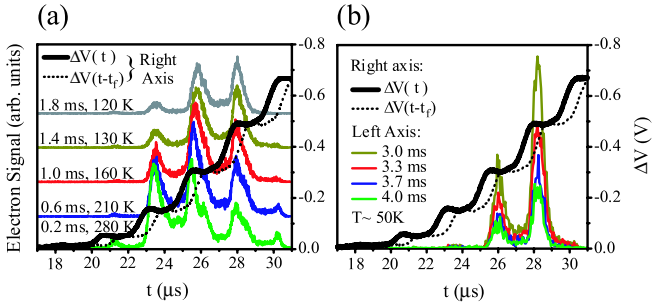

FIG. 4 (color online). (a) Electron extraction signal ($V_{\text{in}} = -2$ V) for delay times up to 1.8 ms. (b) Extraction signal between 3 and 4 ms.

Several sources of error have been considered in evaluating $T_{\parallel}$. First, the extraction ramp occurs over a period of 25 μs. We estimate the time between successive collisions for an electron to be $\Gamma^{-1} = [n\pi b^2 v_z]^{-1} \approx 50\ \mu s$, where $b = e^2/2\pi\epsilon_0 kT_{\parallel}$ is the distance where the Coulomb interaction energy equals the thermal energy in the direction of the magnetic field. Therefore, we do not believe that rethermalization and evaporative cooling during the extraction process significantly affect our measurements. Second, the maxima in the electron signal should coincide with the maxima in the derivative $\frac{d\Delta V}{dt}$. However, in the experiment we observe a time lag of $t_f \approx 1.0$ μs. Using trajectory calculations, we have verified that this time lag reflects the time of flight of an electron from the trap location to the detector. In our temperature calculations, we have accounted for the time-of-flight effect. Third, we ignore the effect of adiabatic cooling during the extraction. In simulations we have established that this omission results in less than 5% error in $T_{\parallel}$. Finally, the positive space charge created by the ions increases the external field required to remove the electrons from the trap, causing an underestimation of the electron temperature. Initially, the width of the space-charge density is about 2.5 mm while the well in which the ions oscillate has a much larger width of about 4 cm. Therefore, the potential the electrons experience resulting from the ionic space charge varies significantly with time. Comparing temperatures obtained for different phases of the trap depth modulation in Fig. 3, we estimate an error of up to 30% caused by neglecting the ionic space-charge potential.

In the following, we discuss possible mechanisms that could result in the observed longitudinal electron cooling. From the temperatures for the data in Fig. 4, the relevant time scale for cooling is ≈ 1 ms. The equilibration of the temperatures parallel and perpendicular to the magnetic field occurs on a similar time scale. For our operating parameters ($B = 3$ T, density $\approx 10^6$–10^7 cm^{-3}, and $T_{\parallel} \approx 100$ K) the equilibration time is on the order of 1 ms [23]. Since the temperatures of the transverse and longitudinal motion are quite different initially in our plasma, this

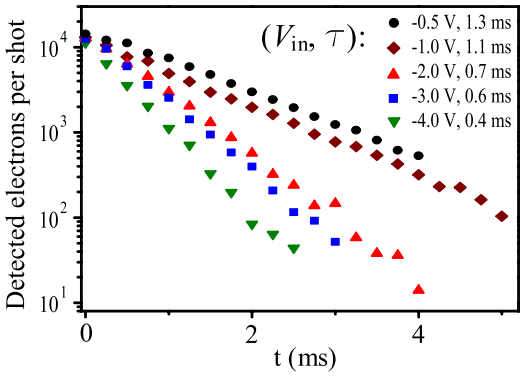

FIG. 5 (color online). Trapped electron number versus time for the indicated values of V_{in}. The $1/e$ lifetimes τ are obtained from fits to the data.

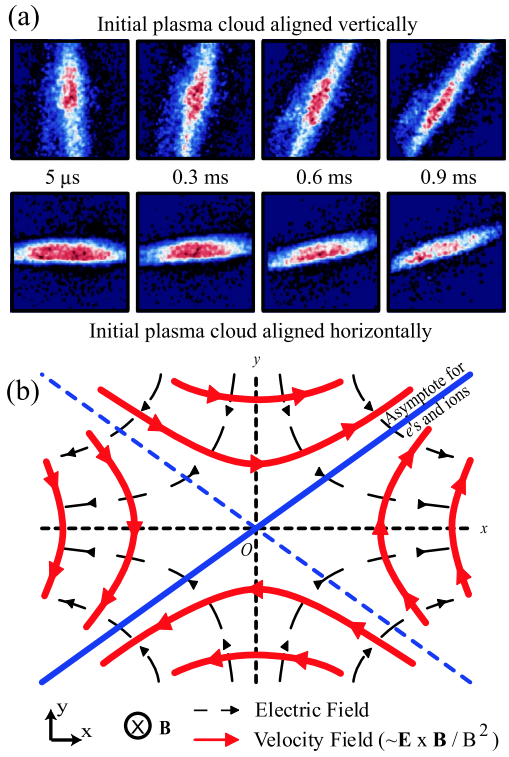

FIG. 6 (color online). (a) Spatial distribution of electrons at indicated extraction delay times. Initially, the plasma is prepared in either a vertical (upper row) or a horizontal (lower row) geometry. (b) Field geometry and resultant $\mathbf{E} \times \mathbf{B}$ drift-velocity field.

relaxation process is likely to contribute to the longitudinal cooling of the trapped electrons. Evaporative cooling is another mechanism which may contribute to the electron cooling. Cyclotron cooling would occur on a time scale of ≈ 0.5 s in our system [23], which is far too slow to account for the observed cooling.

We have measured the electron loss from the nested Penning trap and found $1/e$ lifetimes of order 1 ms (see Fig. 5). To understand the dominant loss mechanism, we investigate the spatial distribution of the electron gas. As the extraction delay increases, the detected electrons approach a diagonal line on the phosphor screen, tilted by $\approx 30°$ from the horizontal line [Fig. 6(a)]. The long-dashed lines in Fig. 6(b) show the electric field in the transverse plane; this field is quadrupolar and arises from the optical apertures near the center of the trap [21] [see also Fig. 1(a)]. Combined with the magnetic field perpendicular to the plane, the quadrupole electric field generates an $\mathbf{E} \times \mathbf{B}$ drift-velocity field [solid lines in Fig. 6(b)] converging to a diagonal line, in agreement with the recorded images. At 2.9 T and estimated transverse electric fields of $\lesssim 50$ mV/cm, the $\mathbf{E} \times \mathbf{B}$ drift velocity is $\lesssim 15$ m/s, which is in agreement with the observed decrease of the electron signal over about 1 ms. For smaller V_{in} (i.e., smaller transverse electric field), the loss rate is reduced accordingly, which explains the observed dependence on V_{in} in Fig. 5. We do not believe that three-body recombination of electrons and ions into Rydberg states causes a significant electron loss for our densities and temperatures.

In summary, we studied the trapping and evolution dynamics of strongly magnetized two-component ultracold plasmas. Ionic and electronic components of the plasmas have been confined over several milliseconds in a nested Penning trap. We observe a periodic modulation of the electron trap depth, caused by a breathing-mode oscillation of the ionic component in the trap. Electron spectra allow us to determine electron temperatures. We have observed cooling in the electron temperature over several milliseconds. The loss of particles from the trap is mostly due to a slow $\mathbf{E} \times \mathbf{B}$ drift motion.

The authors gratefully acknowledge discussions with Jeffrey R. Guest. This work was supported by Atomic, Molecular, and Optical Sciences, Program of the Chemical Sciences, Geosciences and Biosciences Division, Office of Basic Energy Sciences, U.S. Department of Energy.

*Present address: MIT-Harvard Center for Ultracold Atoms, Massachusetts Institute of Technology, Cambridge, MA 02139, USA.
†Present address: Department of Physics, University of California, Berkeley, CA 94720, USA.

[1] T. C. Killian *et al.*, Phys. Rev. Lett. **83**, 4776 (1999).
[2] M. P. Robinson *et al.*, Phys. Rev. Lett. **85**, 4466 (2000).
[3] C. E. Simien *et al.*, Phys. Rev. Lett. **92**, 143001 (2004).
[4] R. S. Fletcher, X. L. Zhang, and S. L. Rolston, Phys. Rev. Lett. **96**, 105003 (2006).
[5] M. S. Murillo, Phys. Rev. Lett. **96**, 165001 (2006).
[6] S. Mazevet, L. A. Collins, and J. D. Kress, Phys. Rev. Lett. **88**, 055001 (2002).
[7] S. G. Kuzmin and T. M. O'Neil, Phys. Rev. Lett. **88**, 065003 (2002).
[8] F. Robicheaux and J. D. Hanson, Phys. Rev. Lett. **88**, 055002 (2002).
[9] T. Pohl, T. Pattard, and J. M. Rost, Phys. Rev. Lett. **92**, 155003 (2004).
[10] T. Pohl, T. Pattard, and J. M. Rost, Phys. Rev. Lett. **94**, 205003 (2005).
[11] M. S. Murillo, Phys. Rev. Lett. **87**, 115003 (2001).
[12] W. M. Itano *et al.*, Science **279**, 686 (1998).
[13] T. B. Mitchell *et al.*, Science **282**, 1290 (1998).
[14] J. R. Guest *et al.*, Phys. Rev. Lett. **94**, 073003 (2005).
[15] J.-H. Choi *et al.*, Phys. Rev. Lett. **95**, 243001 (2005).
[16] M. Amoretti *et al.*, Nature (London) **419**, 456 (2002).
[17] G. Gabrielse *et al.*, Phys. Rev. Lett. **89**, 213401 (2002).
[18] J. L. Roberts *et al.*, Phys. Rev. Lett. **92**, 253003 (2004).
[19] J. Fajans *et al.*, Phys. Rev. Lett. **95**, 155001 (2005).
[20] D. S. Hall and G. Gabrielse, Phys. Rev. Lett. **77**, 1962 (1996).
[21] J. D. Jackson, *Classical Electrodynamics* (John Wiley & Sons, New York, 1999), 3rd ed.
[22] R. G. Greaves and C. M. Surko, Phys. Rev. Lett. **75**, 3846 (1995).
[23] B. R. Beck, J. Fajans, and J. H. Malmberg, Phys. Plasmas **3**, 1250 (1996).